Supporting Information for: The 2015–2017 Pamir Earthquake Sequence: Fore-, Main-, and Aftershocks, Seismotectonics, Fault Interaction and Fluid Processes

Wasja Bloch[1], Sabrina Metzger[1], Bernd Schurr[1], Xiaohui Yuan[1], Lothar Ratschbacher[2], Sanaa Reuter[2], Qiang Xu[3,4], Junmeng Zhao[3,4], Shokhruhk Murodkulov[5], Ilhomjon Oimuhammadzoda[6]

[1]GFZ German Research Centre for Geosciences, 14473 Potsdam, Germany

[2]Geologie, Technische Universität Bergakademie Freiberg, 09599 Freiberg, Germany

[3]Key Laboratory of Continental Collision and Plateau Uplift, Institute of Tibetan Plateau Research, Chinese Academy of Sciences, Beijing 100101, China

[4]CAS Center for Excellence in Tibetan Plateau Earth Sciences, Beijing 100101, China

[5]Institute of Geology, Earthquake Engineering and Seismology, Academy of Sciences, Dushanbe, Tajikistan

[6]Department of Geology under the Government of the Republic of Tajikistan, Dushanbe, Tajikistan

Contents of this file

Corresponding author: Wasja Bloch, wbloch@eoas.ubc.ca now at: Department of Earth, Ocean and Atmospheric Sciences, University of British Columbia, Vancouver, Canada.

Additional Supporting Information (Files uploaded separately)

1. Earthquake catalog
2. Moment tensor catalog

Introduction This supporting information contains the earthquake catalog and the focal mechanism catalog presented in the main body of the text, and additional figures. Please refer to to the Method's section for processing details.

Data Set S1: Earthquake Catalog

seismic_event_catalog.txt

The seismic event catalog presented in the main article.

Columns are:

- Year, Month, Day, Hour, Minute, Second: Time of the seismic event
- Timestamp: Time of the event in seconds since 1. January 1970 (UTC)
- Longitude, Latitude: Coordinates of the event location in degree
- Depth: Depth of the event in kilometer
- P-picks, S-picks: Number of P- and S-wave arrival times used for event location
- revised?: 0 for not manually revised , 1 for revised arrival times
- method: Localization algorithm that yielded the reported location
- RMS: root-mean-square misfit of the *simulps* localization
- Magnitude, uncert: Magnitude of the seismic event and magnitude uncertainty
- type: Magnitude type. M_W moment magnitude; M_L calibrated local magnitude; NEIC moment magnitude published by NEIC.
- Sequence: Letter of the earthquake sequences discussed in the text. A-I: see main text. Z: Below 50 km depth. O: All other events

Data Set S2: Moment Tensor Catalog

moment_tensor_catalog.txt

The moment tensor catalog presented in the main article.

Columns are:

1. Date (YYYY/MM/DD),

2. Time (hh:mm:ss),

3. Longitude (degree),

4. Latitude (degree),

5. Centroid depth (km),

6. Moment magnitude of the event

7. up-up,

8. south-south,

9. east-east,

10. up-south,

11. up-east,

12. south-east elements (10ˆexponent dyne·cm) of the moment tensor (Harvard convention)

13. exponent

14. Strike (degree)

15. Dip (degree)

16. Rake (degree) of the preferred focal mechanism

References

Sippl, C., Schurr, B., Yuan, X., Mechie, J., Schneider, F., Gadoev, M., ... others (2013). Geometry of the Pamir-Hindu Kush intermediate-depth earthquake zone from local seismic data. *Journal of Geophysical Research: Solid Earth*, *118*(4), 1438–1457.

Utsu, T., Ogata, Y., et al. (1995). The centenary of the Omori formula for a decay law of aftershock activity. *Journal of Physics of the Earth*, *43*(1), 1–33.

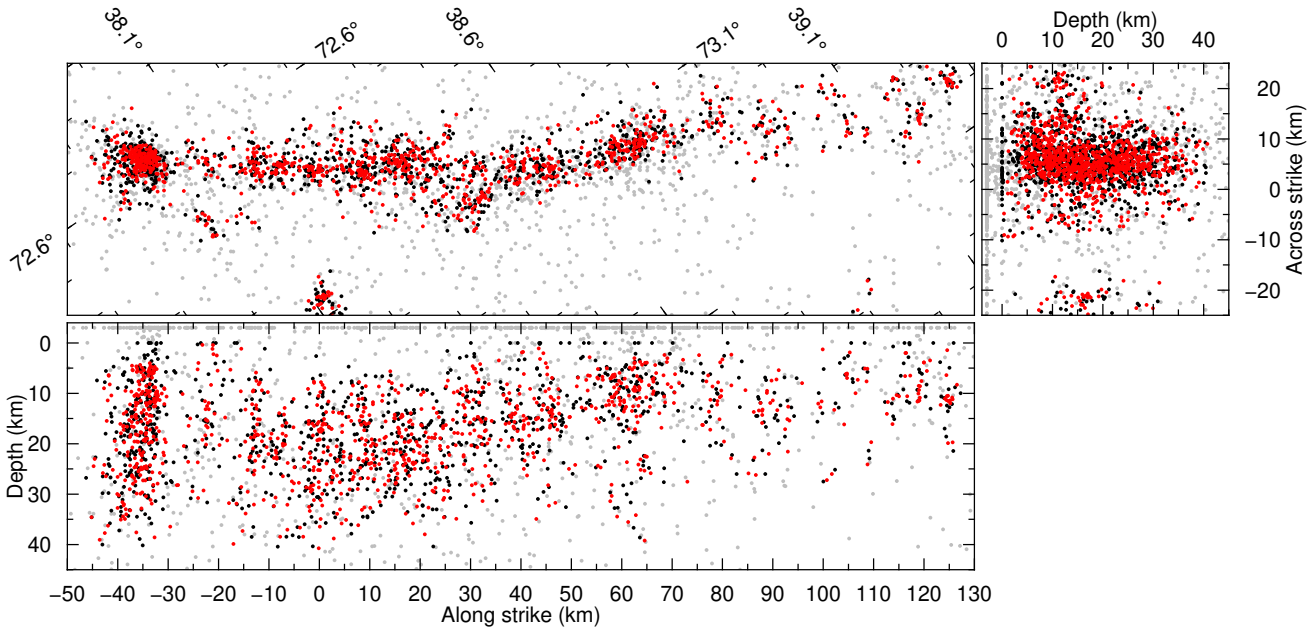

Figure S1. Comparisson of event locations for the Sarez earthquake (Figure 4 of the main text) after the different steps of the event location. Center panel: Map view. Right panel: across-strike profile. Lower panel: along-strike profile. Gray dots are hypocenters which could only be located with *simulps*, but not re-located. Black dots are hypocenters before and red dots after the re-location with *hypoDD*.

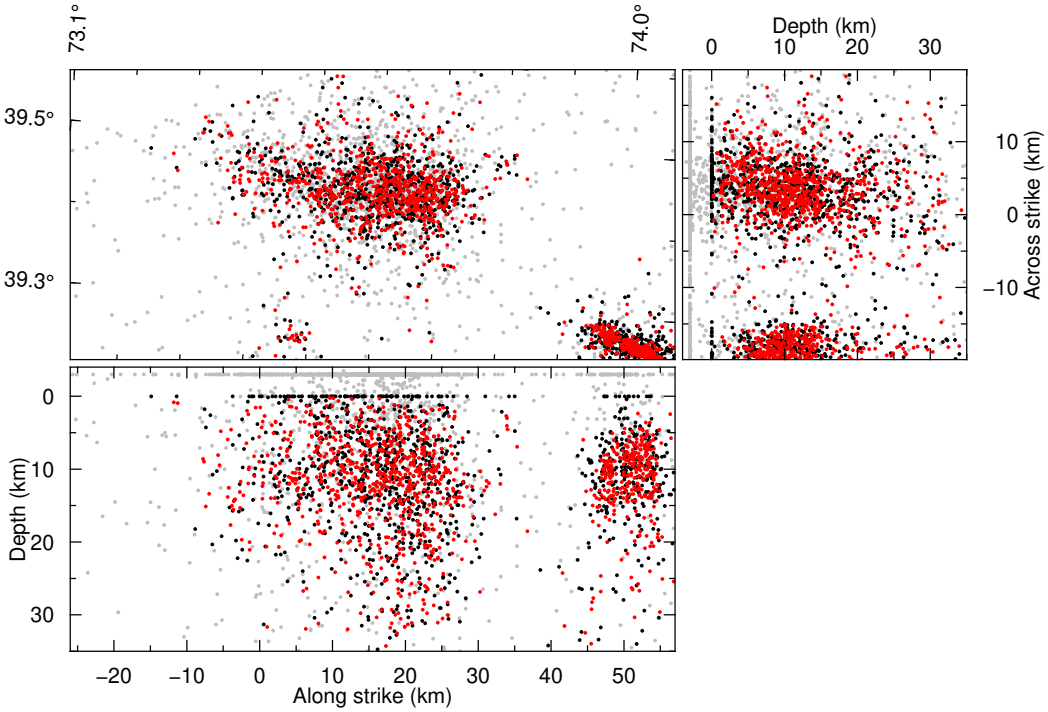

Figure S2. As Figure S1, but for the Sary-Tash earthquake (Figure 6 of the main text).

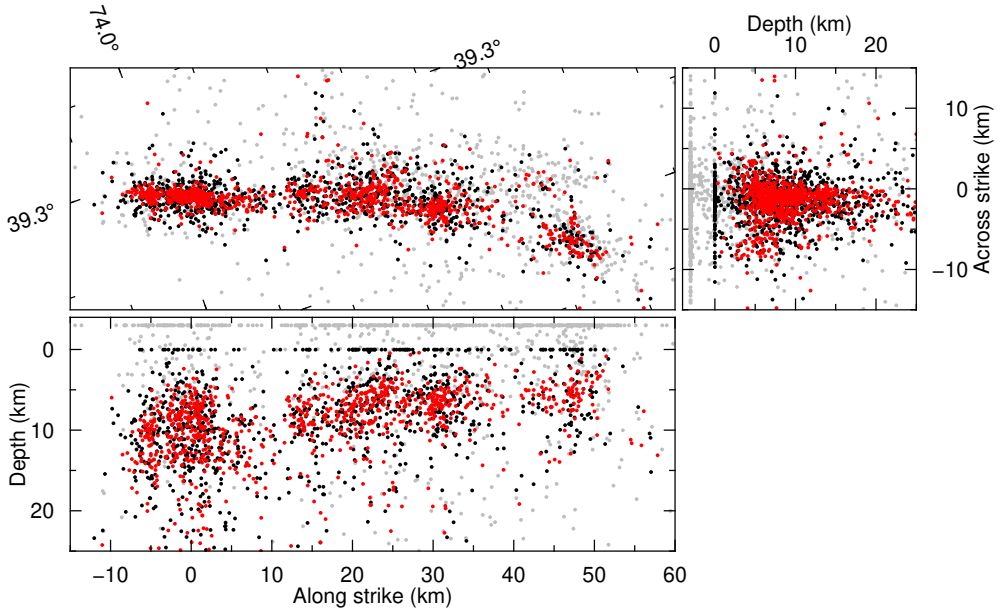

Figure S3. As Figure S1, but for the Muji earthquake (Figure 7 of the main text).

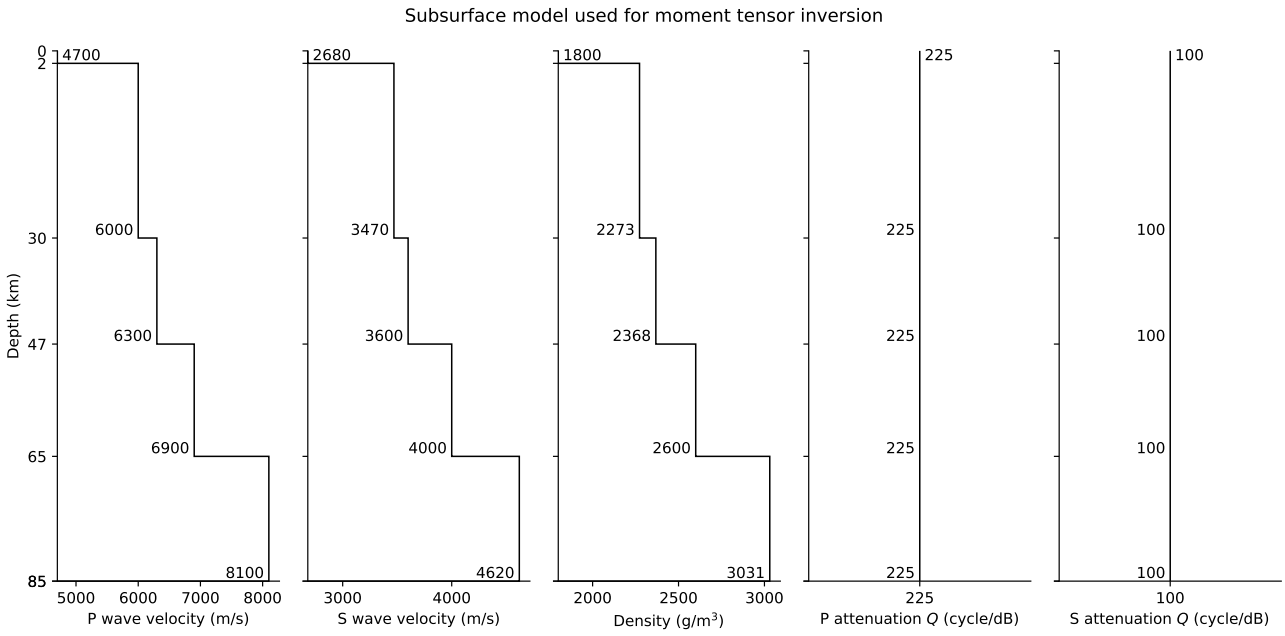

Figure S4. Subsurface model (Sippl et al., 2013) used for the determination of regional moment tensors.

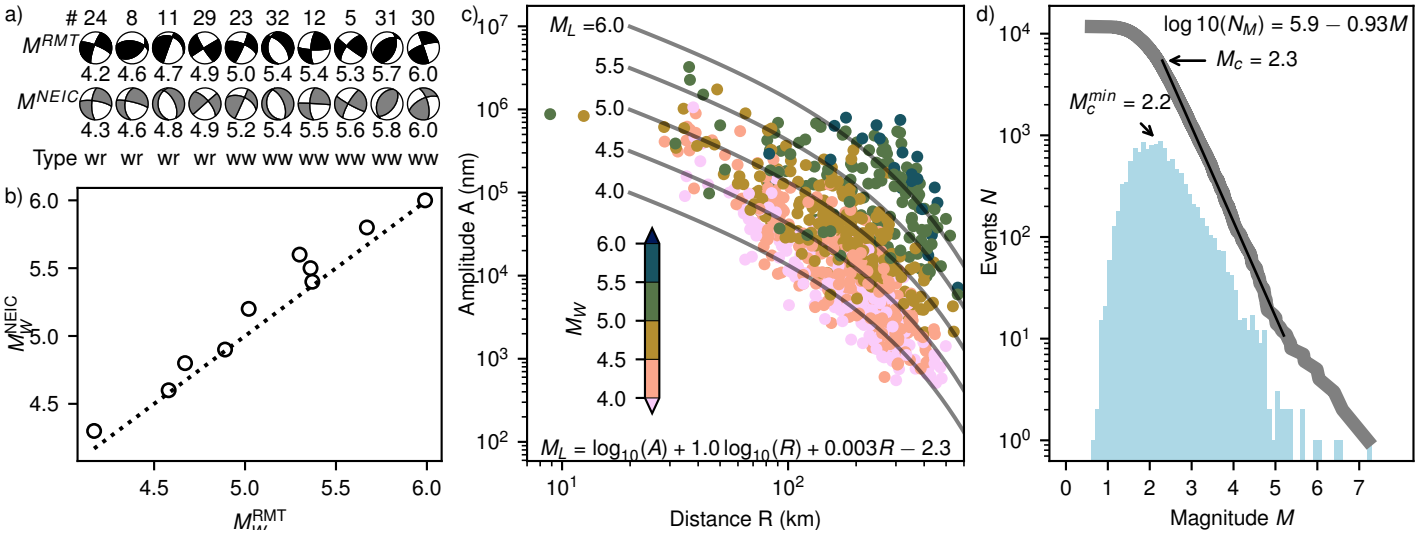

Figure S5. Moment magnitudes of seismic events. Comparison of regional moment tensors (a) and magnitudes (b) with results by NEIC. (wr) regional (ww) W-phase. (c) Calibration of local magnitudes with parameters of Equation 1 of the main text. (d) Magnitude distribution of the entire catalog. Completeness magnitude M_c, and most frequent magnitude M_c^{min}.

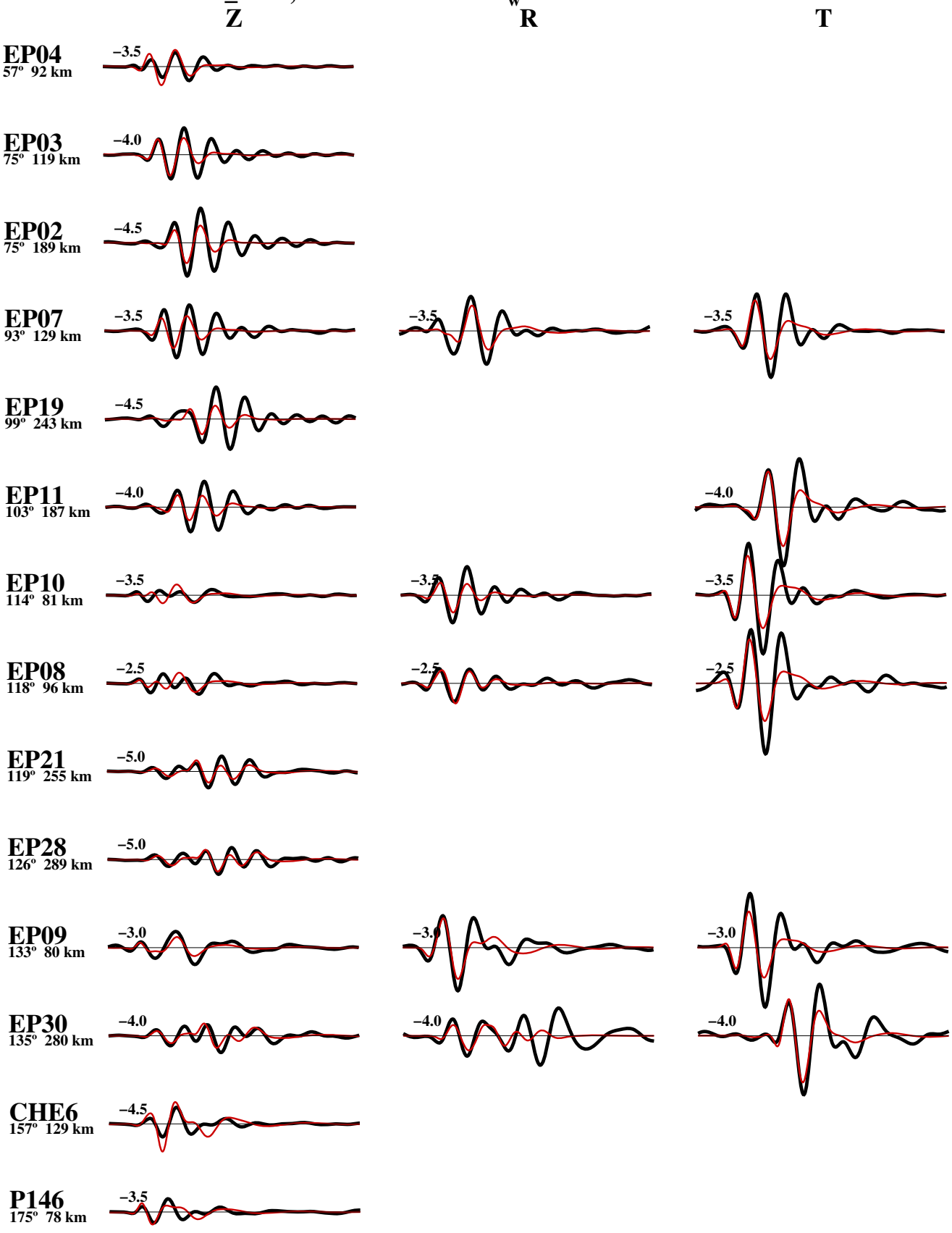
160627_0625, 16/ 6/27 6:25:36 Mw=4.6 20−60s 12km DC:77%
Z
R
T
EP04
57° 92 km
EP03
75° 119 km
EP02
75° 189 km
EP07
93° 129 km
EP19
99° 243 km
EP11
103° 187 km
EP10
114° 81 km
EP08
118° 96 km
EP21
119° 255 km
EP28
126° 289 km
EP09
133° 80 km
EP30
135° 280 km
CHE6
157° 129 km
P146
175° 78 km
−3.5
−4.0
−4.5
−3.5
−3.5
−3.5
−4.5
−4.0
−4.0
−3.5
−3.5
−3.5
−2.5
−2.5
−2.5
−5.0
−5.0
−3.0
−3.0
−3.0
−4.0
−4.0
−4.0
−4.5
−3.5

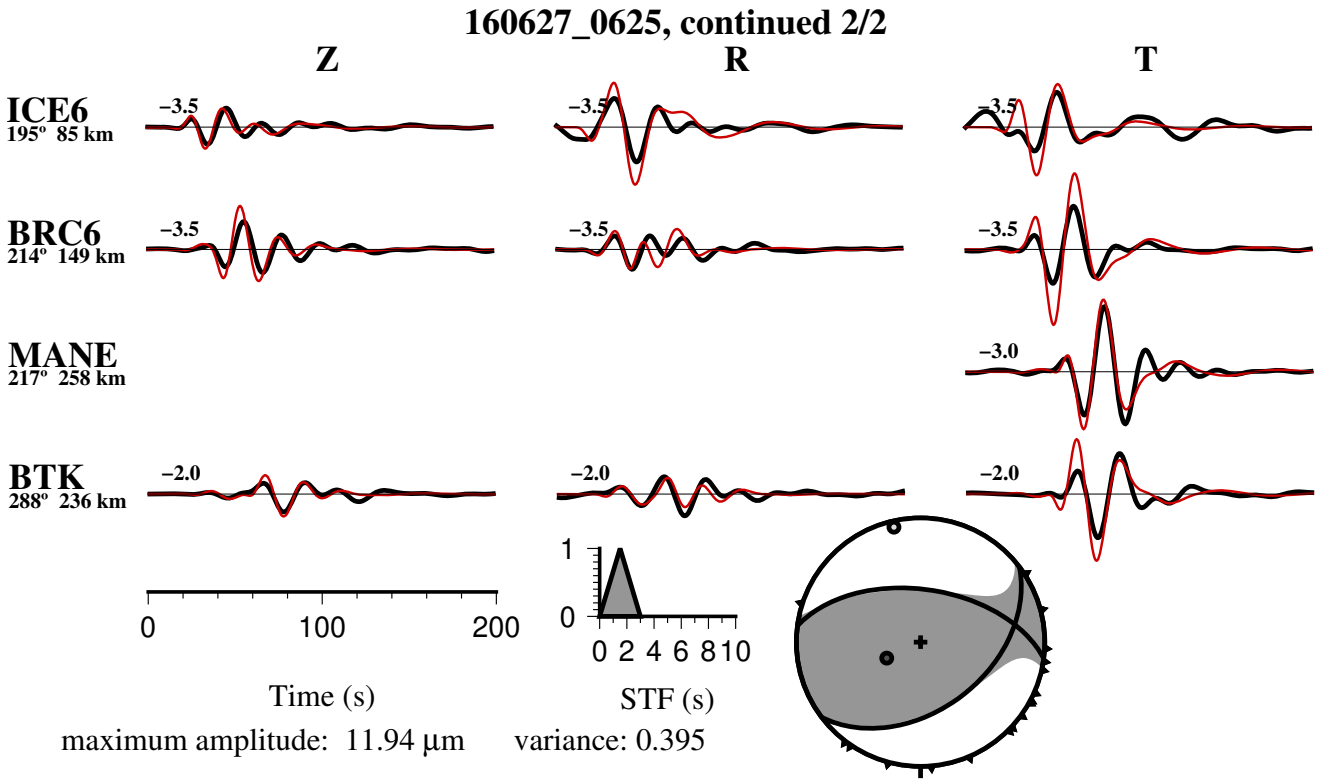

Figure S6. Results of moment tensor inversion for event 8 (Fig. S5), with observed (black) and modeled (red) waveforms for vertial (Z), radial (R) and transvers (T) component on the stations named on the left. Event backazimuth and distance given below station name.

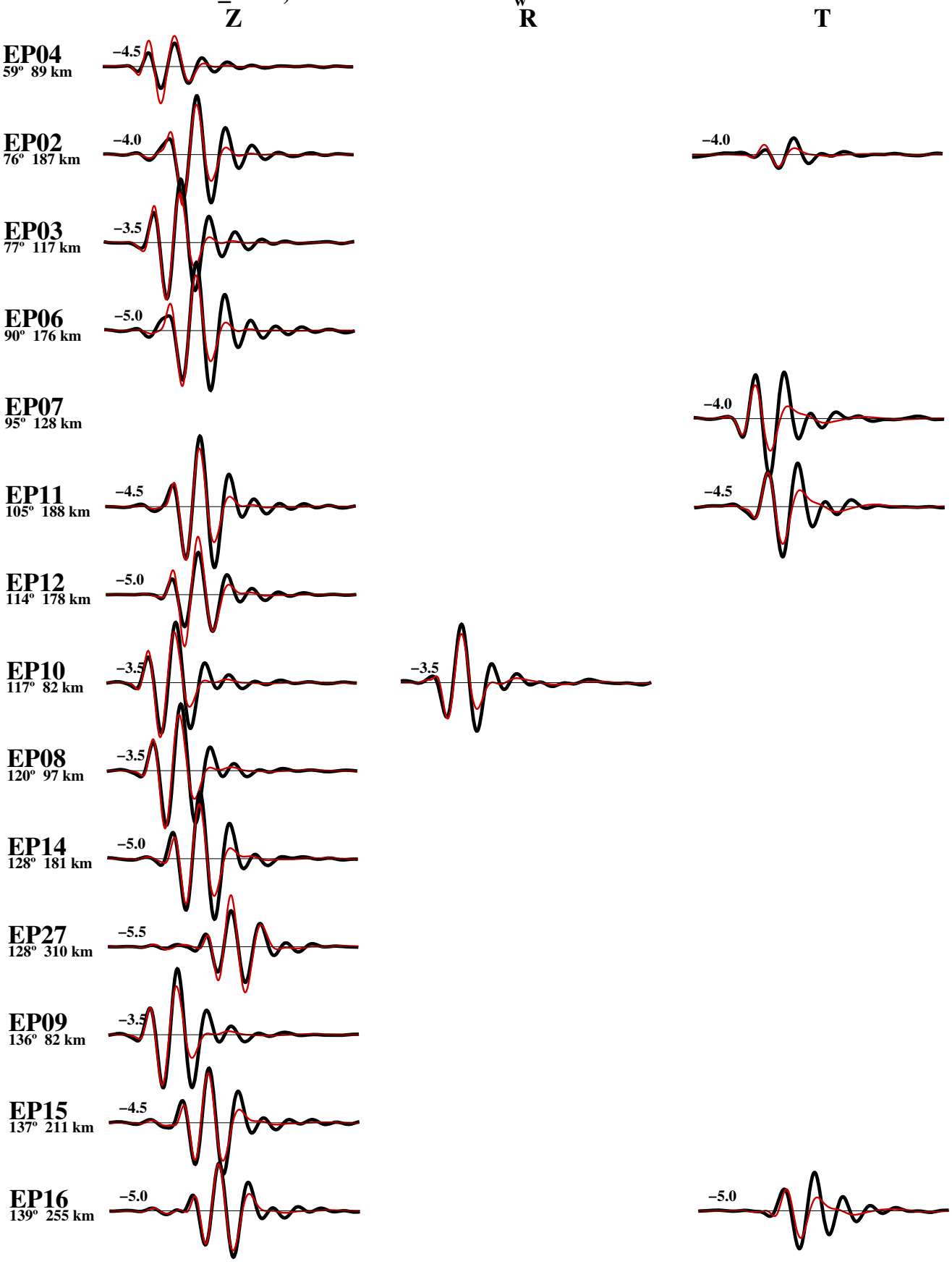
160628_1243, 16/ 6/28 12:43:13 M$_w$=4.7 20–60s 15km DC:81%
Z
R
T
EP04
59° 89 km
−4.5
EP02
76° 187 km
−4.0
−4.0
EP03
77° 117 km
−3.5
EP06
90° 176 km
−5.0
EP07
95° 128 km
−4.0
EP11
105° 188 km
−4.5
−4.5
EP12
114° 178 km
−5.0
EP10
117° 82 km
−3.5
−3.5
EP08
120° 97 km
−3.5
EP14
128° 181 km
−5.0
EP27
128° 310 km
−5.5
EP09
136° 82 km
−3.5
EP15
137° 211 km
−4.5
EP16
139° 255 km
−5.0
−5.0

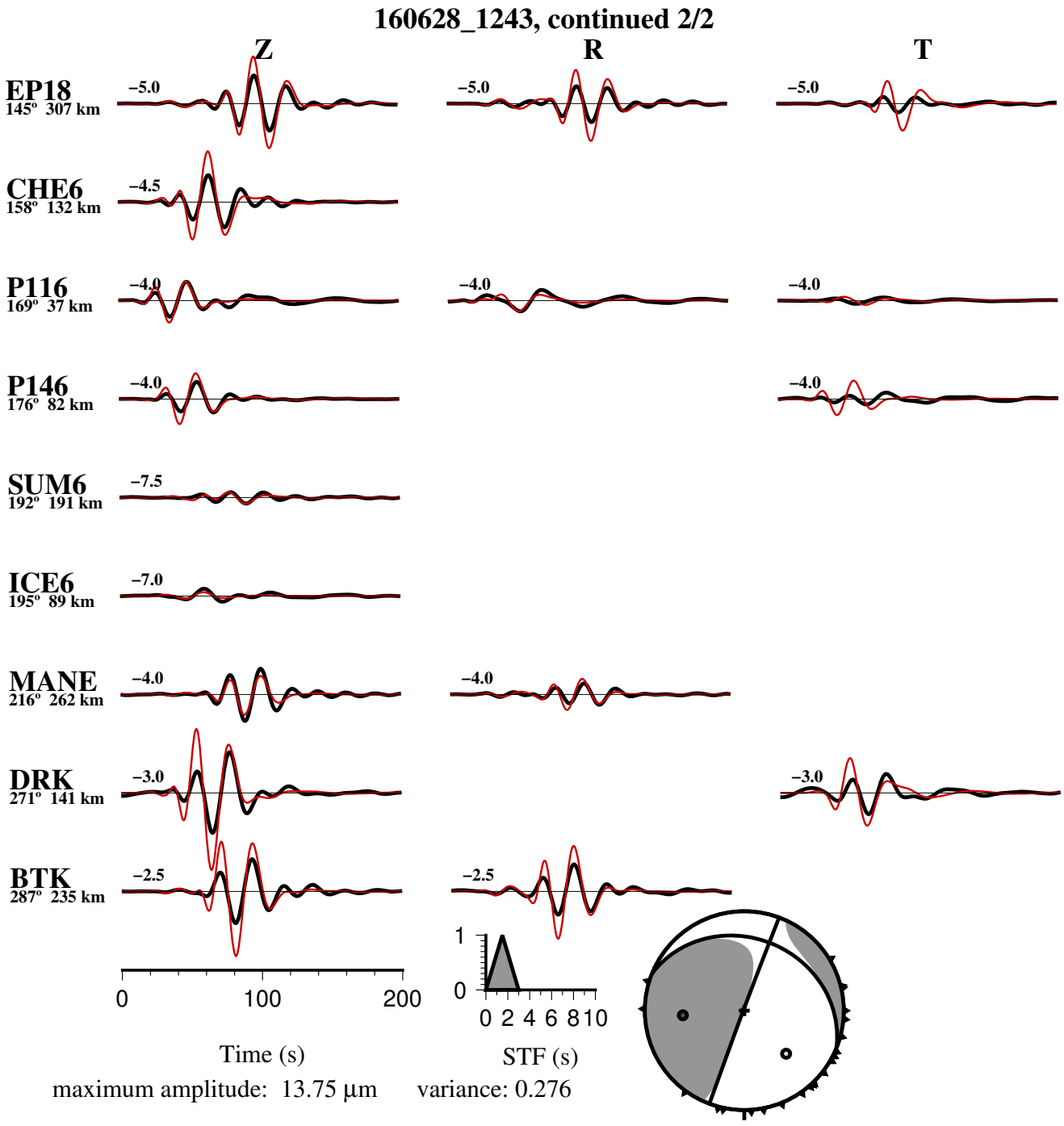

Figure S7. As Figure S6, but for event 11 (Fig. S5).

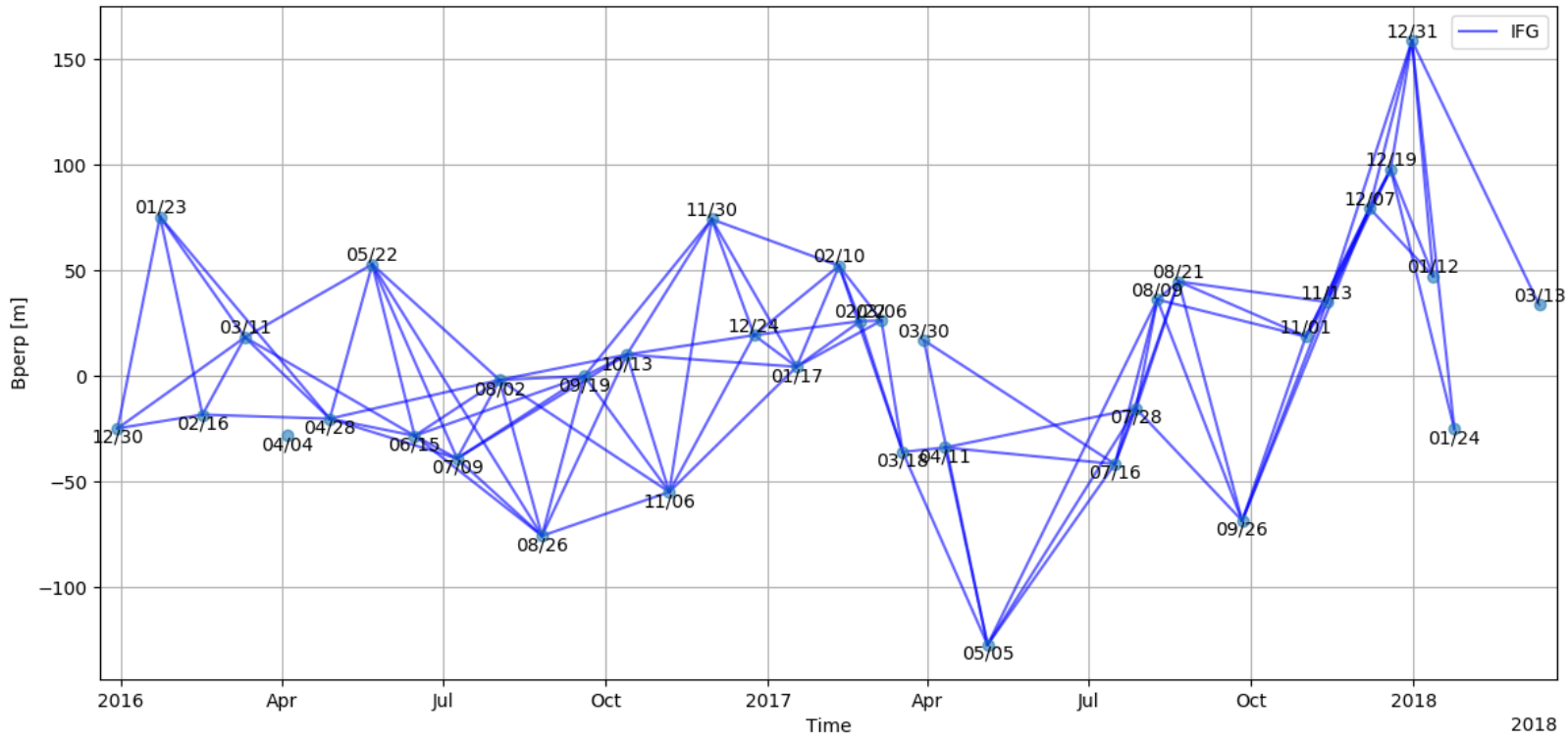

Figure S8. Perpendicular baseline (Bperp) against time for InSAR frame 100A_052 (Figures 4 and S10). Lines indicate combination of acquired images to compute differential interferograms.

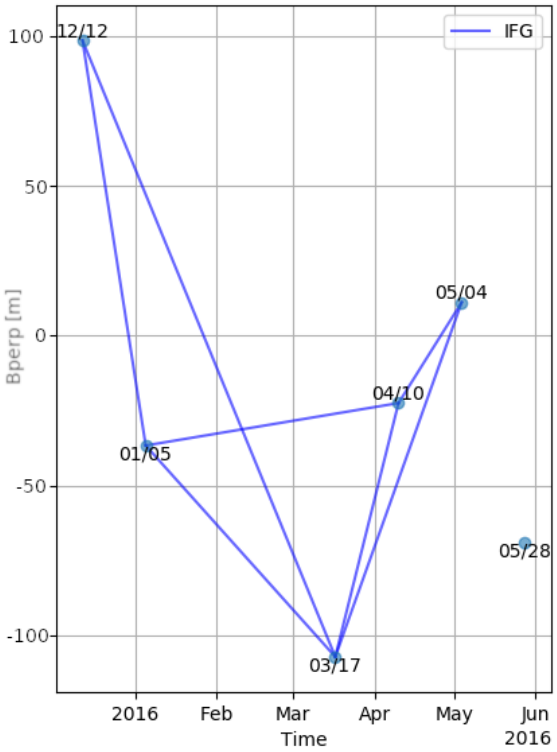

Figure S9. As Figure S8, but for frame 005D_050.

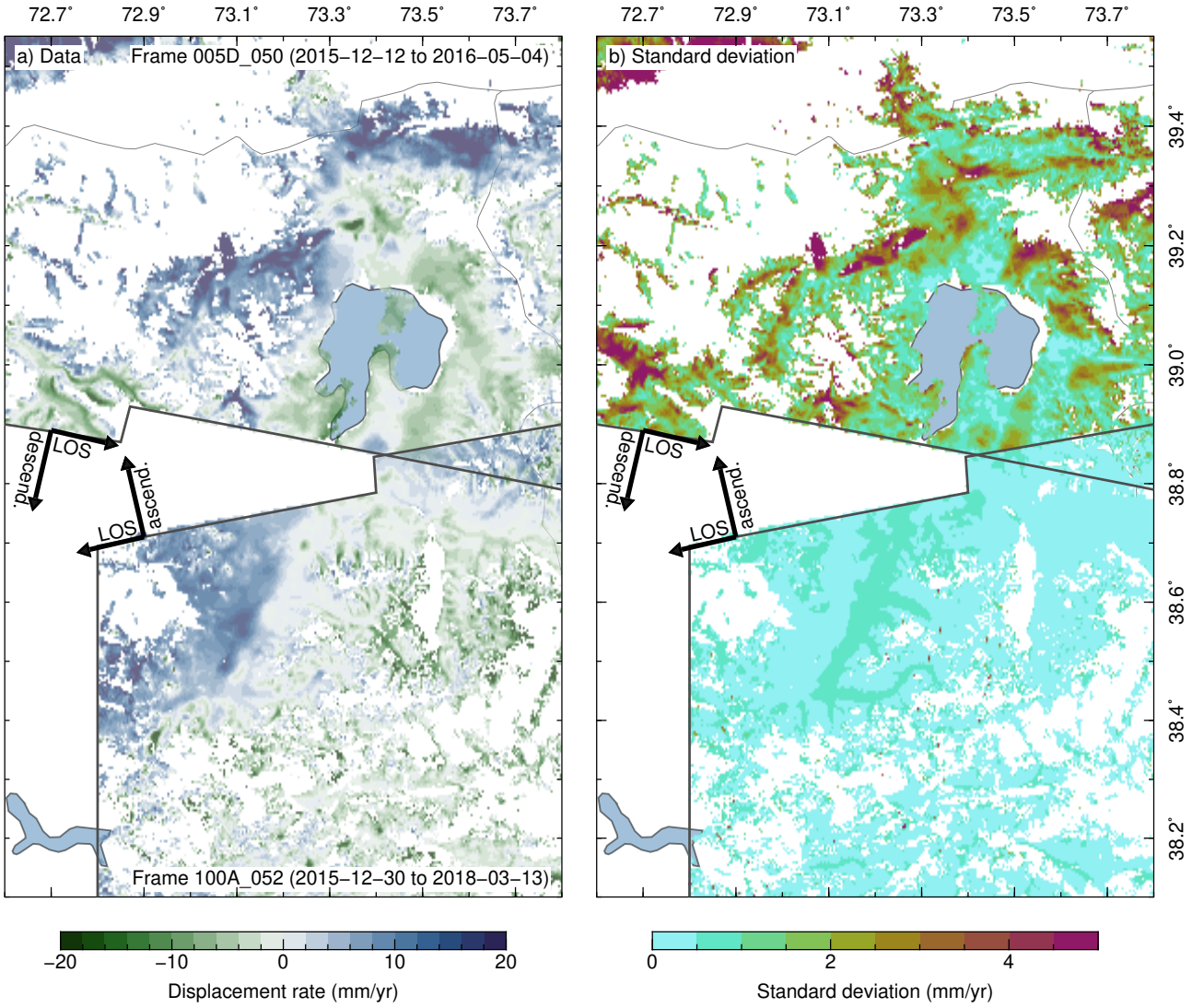

Figure S10. InSAR time series as in Figure 5 of the main text. Left: rate map before conversion to displacement. Right: Nominal uncertainty of displacement rate.

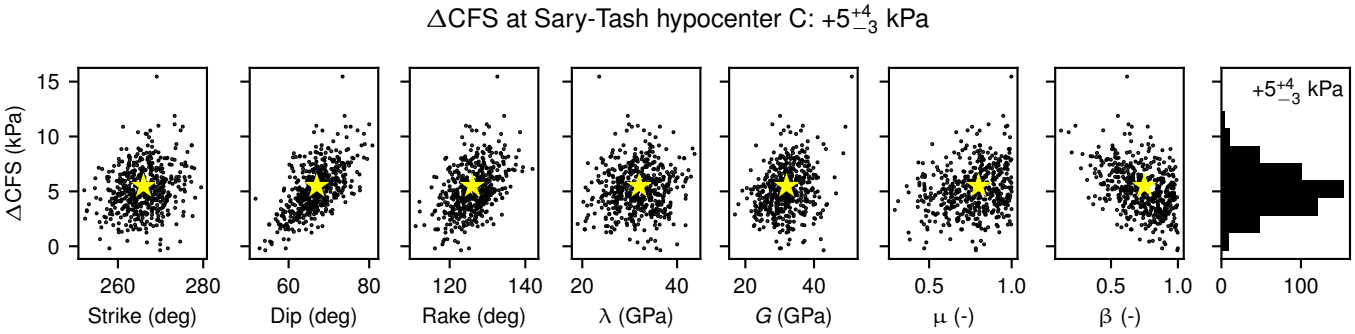

Figure S11. Sensitivity analysis of Coulomb failure stress changes at the Sary-Tash hypocenter *C** due to the Sarez earthquake, postseismic slip on the Sarez fault and foreshock *e'*. Contributions (from left to right) of normal distributed variations around the preferred values (stars)of receiver fault's strike, dip and rake (with a standard deviation of 5°), Lamé's parameters λ and G (standard deviation of 5 GPa), friction coefficient μ, and Skempton's parameter β (standard deviation 0.2, ensuring [0, 1] range). Resulting median, 5% and 95% quantiles under the assumption of input uncertainties.

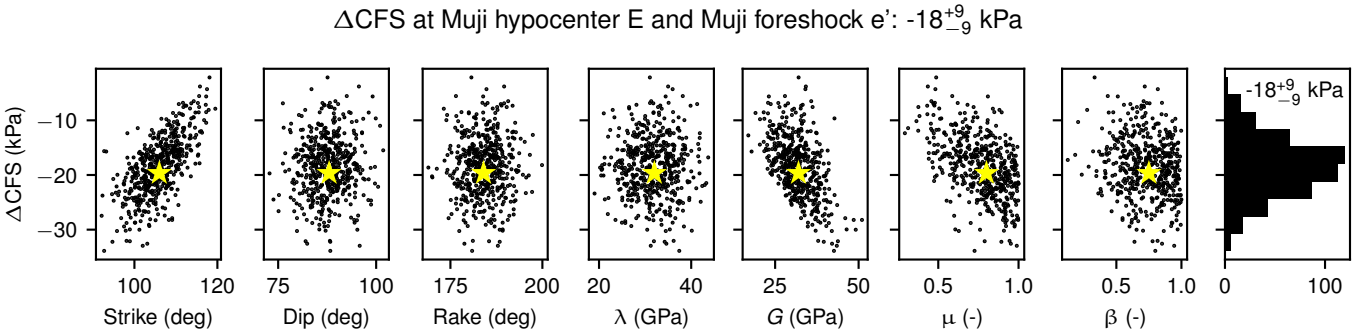

Figure S12. Sensitivity analysis of Coulomb failure stress changes as in Figure S11, but due to the Sarez and Sary-Tash earthquakes at the Muji mainshock *E** or Muji foreshock *e'* hypocenter, both of which yield the same results within 100 Pa.

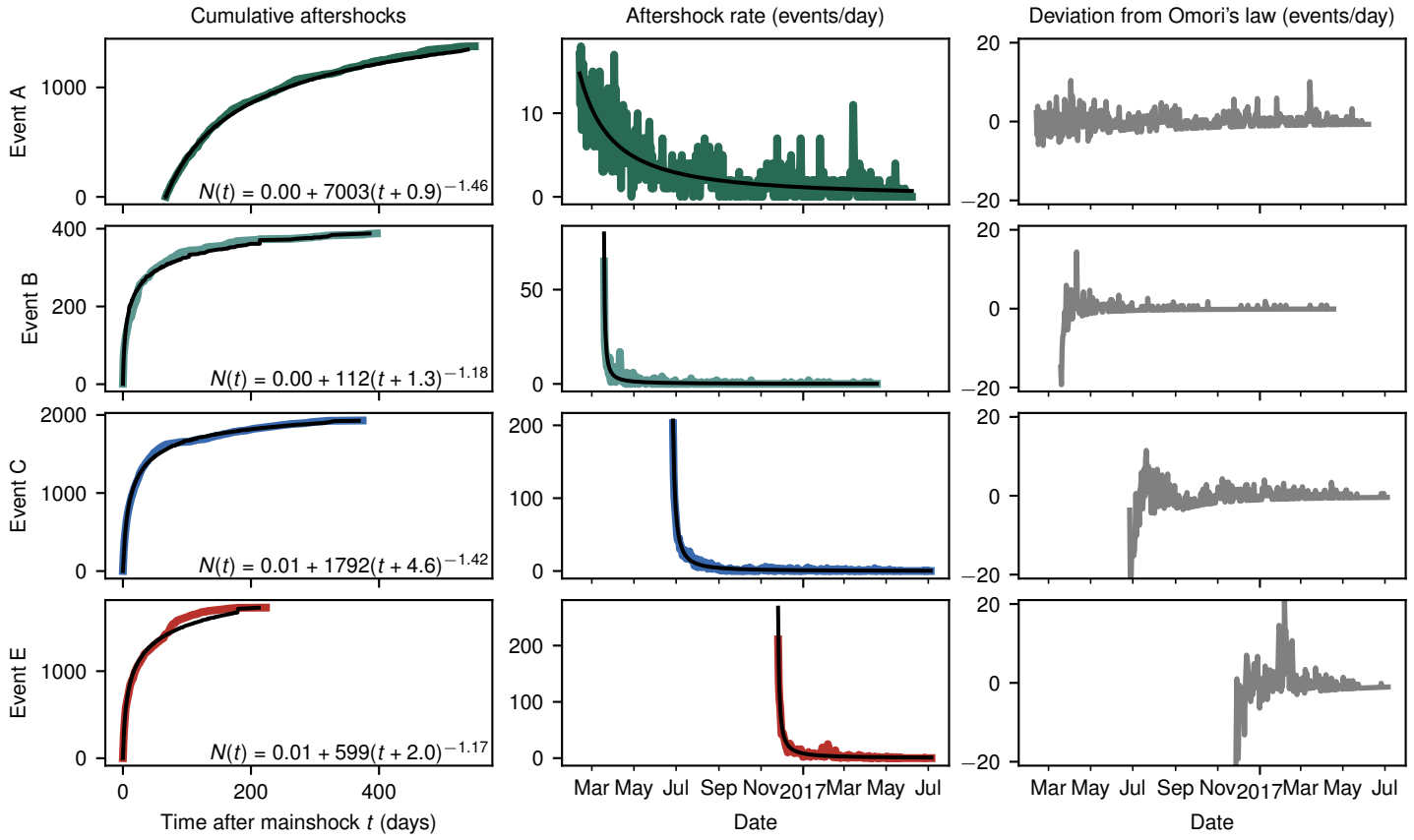

Figure S13. Aftershock characteristics of mainshock vicinities *A*, *B*, *C*, and *E*. Left column: Cumulative aftershocks after the mainshock (*A** only shown after installation of 8H network) and parameters of modified Omori's Law (Utsu et al., 1995). Middle column: Aftershock rate over time. Right column: Deviation of aftershock rate from Omori's law over time. Even though time intervals of increased aftershock activity exist, they to not correlate with each other in between earthquake sequences.

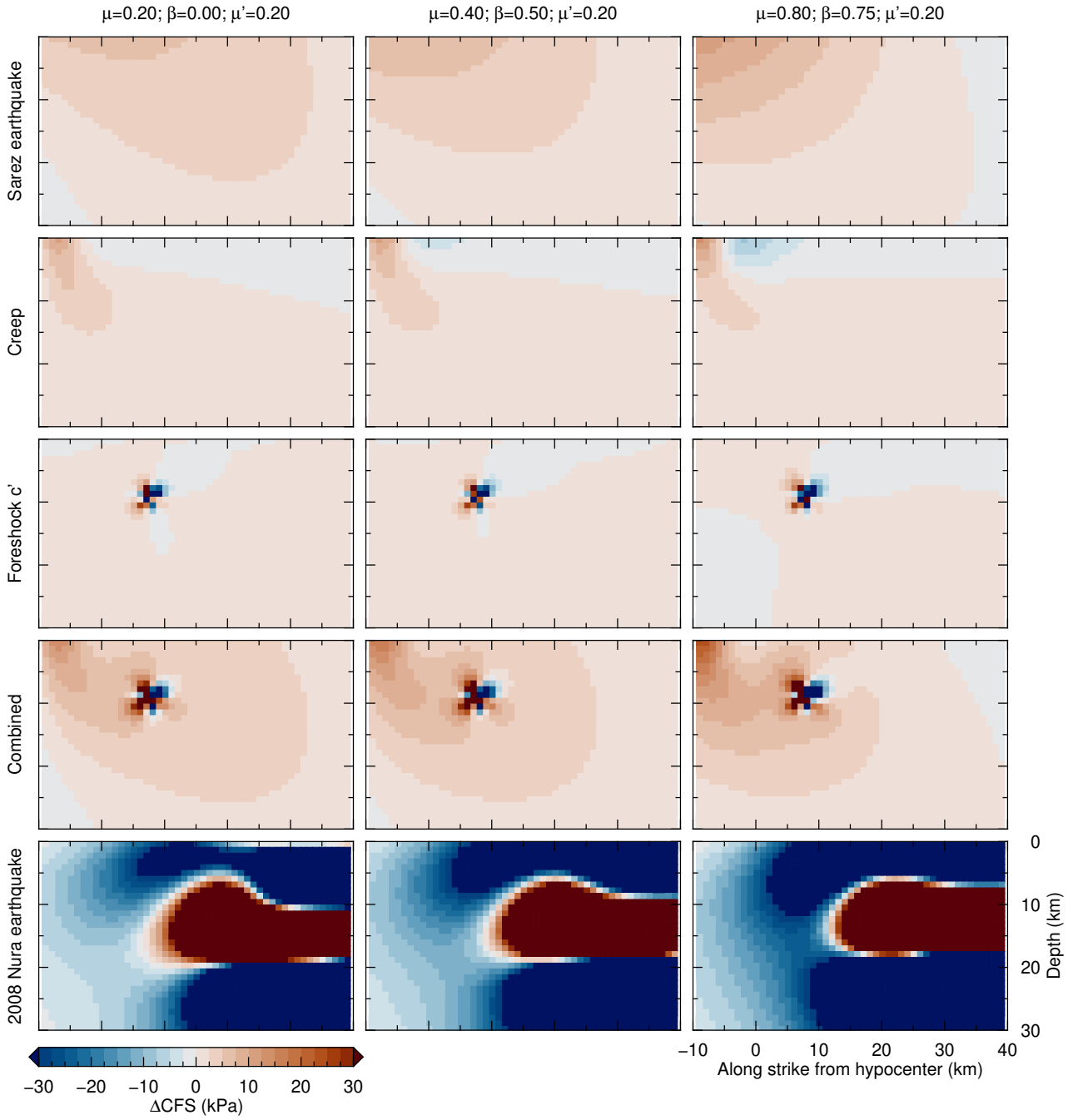

Figure S14. Contributions of distinct stress sources to the change in Coulomb failure stress (ΔCFS) on the fault plane of the Sary-Tash earthquake in dependence of friction (μ) and Skempton's parameter (β) under constant apparent friction (μ').

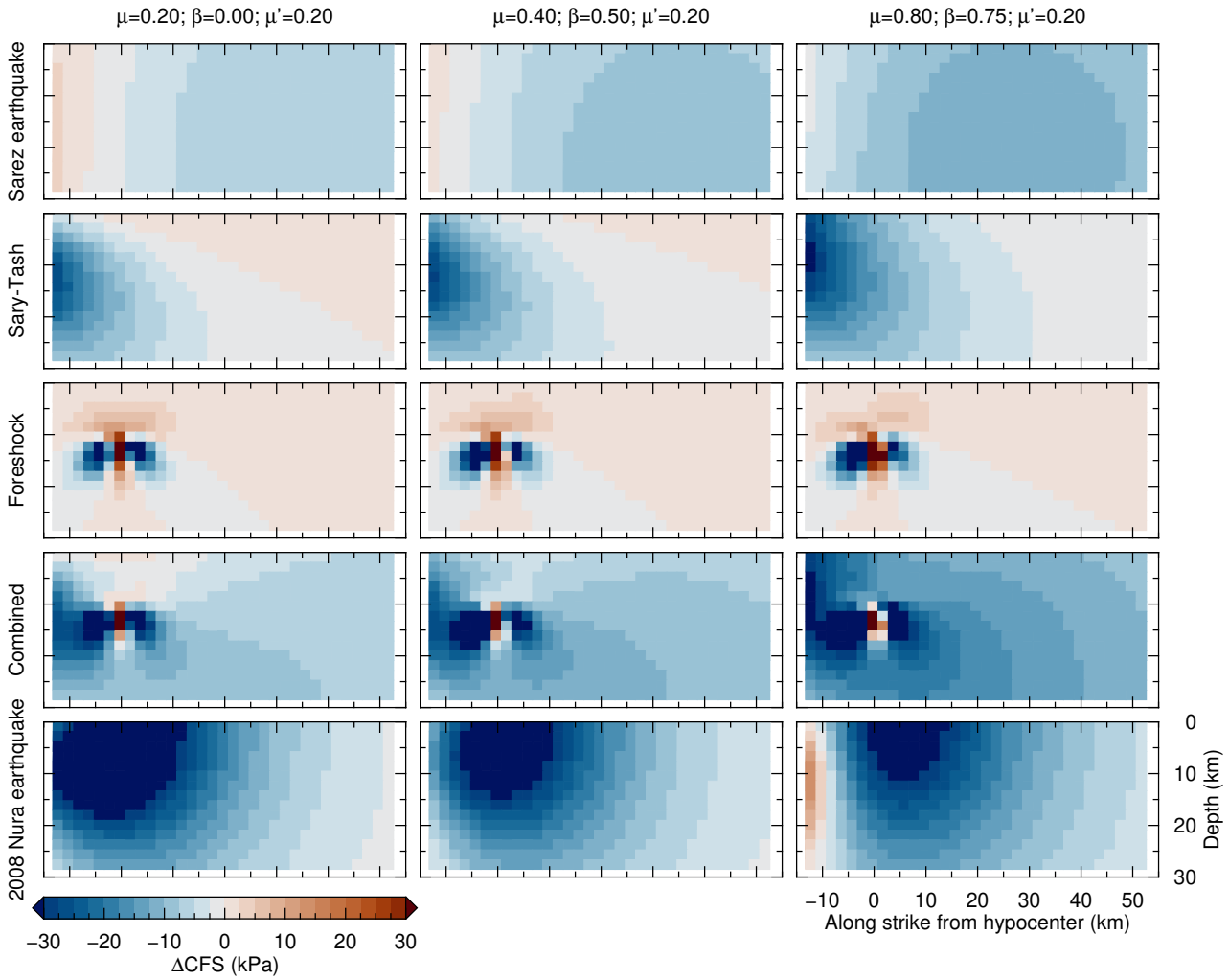

Figure S15. As Fig. S14, but for the Muji earthquake.

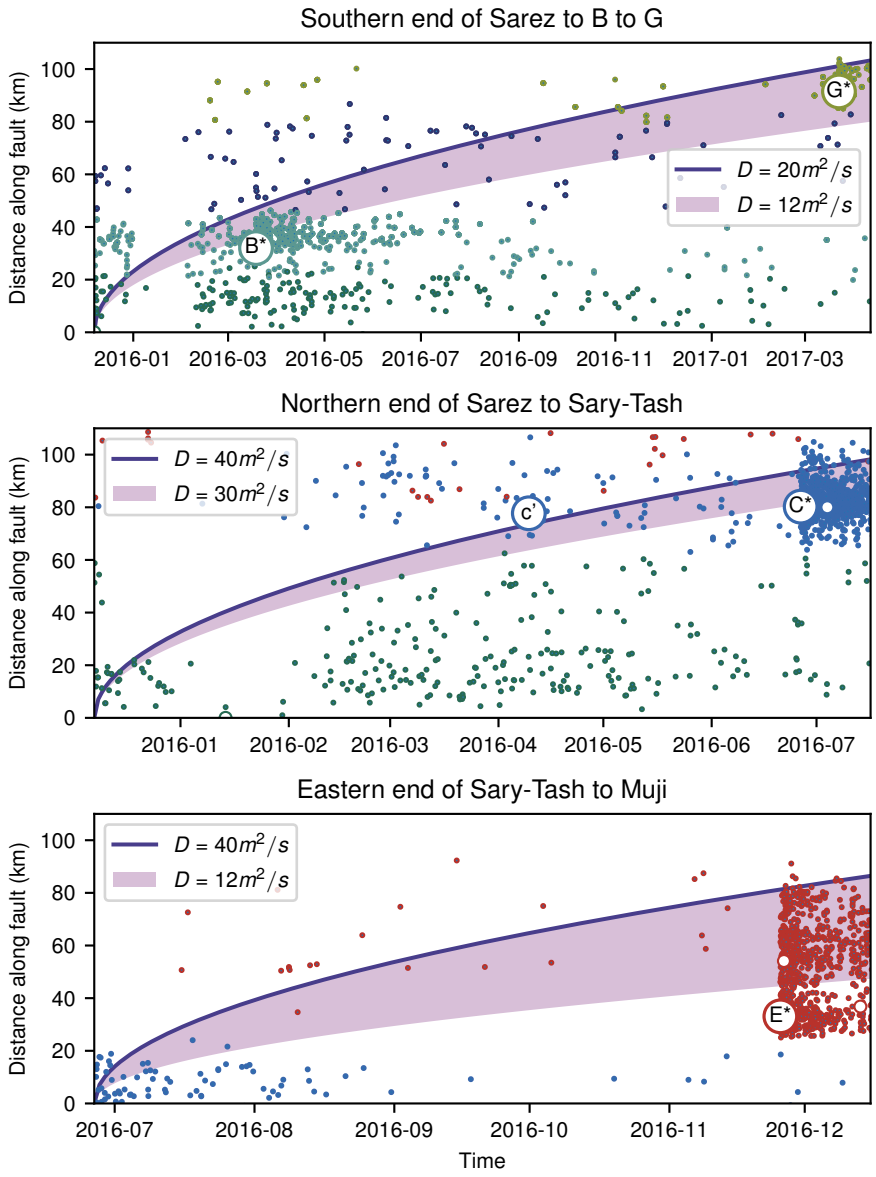

Figure S16. Spatio-temporal evolution of seismicity along the (top) southern continuation of the SKFS; (middle) northern continuation of the SKFS; (bottom) continuation of the MPTS into the Muji fault. D according to Equation 8 of the main text.